JOURNAL OF MATERIALS SCIENCE 33 (1998) 3377–3389

Microstructure-related fracture behaviour of injection moulded short fibre reinforced polyarylamide in dry and wet states

Z. A. MOHD ISHAK, U. S. ISHIAKU
School of Industrial Technology, Universiti Sains Malaysia, 11800 Pulau Pinang, Malaysia

J. KARGER-KOCSIS
Institute for Composite Materials Ltd, University of Kaiserslautern, P.O. Box 3049, D-67663 Kaiserslautern, Germany
E-mail: zarifin@usm.my

The fracture behaviour of injection moulded polyarylamide (PAR) composites containing 30, 50 and 60 wt% glass and 30 wt% carbon fibres has been investigated in both dry and wet states. Kinetics of moisture absorption study revealed that PAR and its composites exhibit Fickian behaviour. The incorporation of short fibres into a PAR matrix has resulted in the reduction of both maximum moisture content (M_m) and diffusion coefficient (D). The fracture mechanical characterization of the various materials was evaluated by using notched compact tension (CT) specimens. Testing was performed as a function of temperature ($T = -40$, 20 and 80 °C) and crosshead speeds (v = 1 and 1000 mm min^{-1}) on as received (AR) specimens. The influence of water uptake due to the hygrothermal ageing (HA) process on residual fracture performance was also studied. The combined action of moisture-induced plasticization of the PAR matrix and interfacial degradation has been concluded to play a significant role in controlling the fracture behaviour of the (HA) composites. The residual fracture properties of both neat PAR and its composites are almost fully recovered in the case of redrying (RD). Failure mechanisms of both the matrix and the composites, assessed by fractographic studies in a scanning electron microscope (SEM) are discussed.

1. Introduction

Polyarylamide (PAR) is a relatively new semi-crystalline engineering thermoplastic which is introduced as a matrix material in the production of short fibre reinforced thermoplastics (SFRTP) composites. It is produced via a polycondensation process involving a combination of m-xylene diamine and adipic acid. The presence of aromatic groups in its molecular structure has resulted in the material possessing excellent mechanical, physical, thermal and chemical properties. These factors, combined with the ease of processing using rapid, inexpensive processes such as extrusion and injection moulding, have positioned PAR as a suitable candidate to be used in electronics, automobiles and high temperature composites [1].

Despite its extensive potential applications, surprisingly, few studies on PAR and its composites have been made. Recently, Hadout and Villoutine [2] carried out an investigation on fibre orientation in injection moulded short glass fibre PAR composites. They studied the effects of moulding conditions and flow geometry on fibre orientation. However, to date, there are few published reports on the mechanical properties of PAR and its composites. Recently, Czigany *et al.* [3] characterized the failure mode of injection moulded short fibre reinforced PAR composites using acoustic emmision (AE) and fractography techniques. They reported that both techniques are suitable for clarifying the failure mode and for discriminating between different failure mechanisms.

It is known that the mechanical properties of SFRTPs are governed by complex interactions of internal or microstructure related parameters such as types of matrix, types and volume fraction of fibres, fibre aspect ratio and fibre orientation distributions and fibre-matrix interface. In addition, there are other external parameters that need to be considered and these are the rate and mode of testings and also environments. It is the objective of the present paper to investigate the fracture behaviour of PAR and its short fibre composites in terms of both the stated parameters. Previous studies by Karger-Kocsis and Friedrich have indicated that there exist basic relationships between the process-dependent microstructure and the failure behaviour of short fibre composites based on semi-crystalline thermoplastics

such as polyamide 6.6 [4], polyetheretherketone [5] and polyphenylene sulfide [6]. Thus this paper serves to establish further understanding of the fracture behaviour of PAR and its composites as a function of microstructure. As far as external parameters are concerned, the effects of temperature, strain-rate and water absorption on the materials fracture toughness will be investigated. The effect of water is of particular interest because PAR, like polyamides, contains amide groups which are susceptible to moisture attack. In the case of polyamide 6.6 and its short carbon fibre composites, for instance, the water molecule has been proven to act as a plasticizer forming complexes with the amide groups in a reversible way. This plasticization leads to a reduction in the glass transition temperature [7]. Thus, it is also the aim of the present study to investigate the role of aromatic groups in PAR with regard to water uptake and subsequently to illustrate how water absorption influences the fracture behaviour of PAR and its composites.

2. Experimental

2.1. Materials

Neat PAR and PAR composites reinforced with 30, 50 and 60 wt % of glass fibres and 30 wt % carbon fibres were supplied by Solvay SA, Brussels, Belgium in the form of rectangular film-gated injection moulded plaques of dimensions 120 mm × 120 mm × 3 mm.

2.2. Sample characterization

The melting and crystallization behaviour of the moulded samples were analysed using a Mettler DSC 30 differential scanning calorimeter with a TC 11 TA processor. The samples was scanned from −50 to 350 °C at two heating rates, i.e. 2 and 20 °C min^{-1}. Analysis was performed under a nitrogen purge at a flow rate of 10 ml min^{-1} to prevent oxidative degradation. The degree of crystallinity, X_c, was calculated assuming a heat of fusion of the perfectly crystalline PAR sample the same as that of the pure polyamide 6.6 crystal, which is 130 J g^{-1} [4].

The fibre content in the composite samples was determined using a Mettler M3 thermogravimetry analyser (TGA) with a TC 11 TA processor. The samples were placed in an aluminium crucible and scanned from room temperature to 600 °C at a heating rate of 20 °C min^{-1}. Analysis was performed under a nitrogen purge at a flow rate of 10 ml min^{-1} to prevent oxidative degradation. Once the temperature reached 600 °C, the samples was kept at this temperature in air for 10 min. This procedure is essential to ensure that the PAR matrix is fully decomposed. The fibre content was calculated using the step analysis available in Mettler Graphware data evaluation software. The accuracy of the glass fibre content determined by the TGA technique was checked using the resin burn-off method. The reinforced samples were pyrolysed in a muffle furnace by gradually increasing the temperature to 600 °C and maintaining at this temperature for 1 h. As for the carbon fibre composites, the volume fraction of fibres was measured by chemical digestion of the matrix.

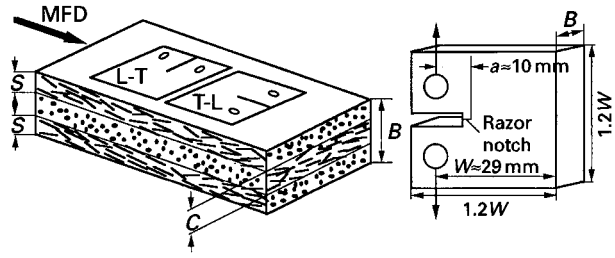

Figure 1 Machining and designation of the CT-specimens used along with a schematic of the fibre layering due to injection moulding.

The microstructure of the moulded plaques was characterized by the fibre layering (ratio of the core layer to the specimen thickness, C/B). The C/B ratio was determined by considering the fracture surface of broken compact tension (CT) specimens in the scanning electron microscope (SEM). The skin layer, S was defined as the layer in which the fibres was aligned predominantly parallel to the mould filling direction, (MFD). The core layer, C was the remainder of the specimen (cf. Fig. 1).

2.3. Kinetics of moisture absorption

Rectangular specimens (of dimensions 120 mm × 10 mm × 3 mm) were dried at 80 °C in a vacuum oven until a constant weight was attained prior to immersion in water in a thermostated stainless steel water bath at 90 °C. Weight gains were recorded by periodic removal of the specimen from the water bath and weighing on a balance with a precision of 1 mg. The percentage gain at any time t, M_t as a result of moisture absorption, was determined by:

$$M_t(\%) = (W_w - W_d)/W_d \times 100 \quad (1)$$

where W_d and W_w denote, respectively, weight of dry material (i.e. the initial weight of material prior to exposure to the environment) and weight of moist material.

The percentage equilibrium or maximum moisture absorption, M_m, was calculated as an average value of several consecutive measurements that showed no appreciable additional absorption.

The weight gain resulting from moisture absorption can be expressed in terms of two parameters, the diffusion coefficient or diffusivity, D, and the maximum moisture content, M_m, as [8]:

$$\frac{M_t}{M_m} = 1 - \frac{8}{\pi^2}\exp\left[-\left(\frac{Dt}{h^2}\right)\pi^2\right] \quad (2)$$

where h is the thickness of the sample.

2.4. Fracture

Compact tension (CT) specimens (notch length, a = 10 mm; free ligament width, W = 29 mm) were machined from the injection moulded plaques as

indicated in Fig. 1. Specimens with an initial notch cut parallel or longitudinal to MFD are designated as T-L whereas those with a notch perpendicular or transverse to the MFD are labelled as L-T, according to the ASTM E 616-81 standard. Thus, in the T-L and L-T CT specimens, their loading occurred transverse (T) and longitudinal (L) to the MFD, respectively. In order to avoid edge effects, the samples were taken from the central position of the plaques, and notches were made in such a way that their tips pointed (more or less) towards the centre of the plate. Prior to the static loading tests, the notch of the CT specimen was sharpened by a fresh razor blade.

Fracture toughness determinations were carried out on a Zwick 1445 type testing machine. Measurements were conducted at different temperatures ($T = -60$, 20 and 80 °C) achieved by the use of a thermostatically controlled chamber attached to the testing machine. A crosshead speed, v of 1 mm min^{-1} was used throughout. At 20 °C, additional tests were performed at a crosshead speed of 1000 mm min^{-1} to investigate the effect of testing speed or strain rate.

Because of the hygroscopic nature of PAR, the machined CT specimens were placed in a vacuum oven at 100 °C for 8 h prior to testing. After removal from the oven, the specimens were allowed to cool to room temperature inside a desiccator to maintain a standard moisture content for all specimens. These specimens are then regarded to be in the as-received (AR) state.

The study on the effect of moisture uptake on the fracture properties was carried out on both neat PAR and its composites. The specimens were hygrothermally aged (HA) or conditioned to 100% RH at 90 °C prior to testing. Once the water uptake in the specimens has reached a saturation limit, the fracture test was carried out at room temperature using a crosshead speed of 1 mm min^{-1}. Testing of redried (RD) samples was also performed under the same condition. The purpose of this additional test was to elucidate the nature of attack of water on the samples.

The fracture toughness (K_c) and fracture energy (G_c) were calculated in accordance with the recommendation of the protocol of the ESIS TC-4 (1990). In all cases, three CT specimens of each material were tested.

2.5. Fractography studies

The failure mode of the fractured CT specimens was examined using a Jeol JSM 5400 scanning electron microscope (SEM). SEM micrographs were taken at 25 kV acceleration voltage at various magnifications. Prior to the SEM observations the fractured parts of the specimens were mounted on aluminium stubs and were sputter coated with a thin layer of gold to avoid electrical charging during examination. The fracture surface was examined from the initial razor cut precrack up to the point where unstable fracture occurred. In addition, the topology of the surface crack path on partially broken CT-specimens was also studied using SEM.

3. Results and discussion

3.1. Sample characterization

Fig. 2 shows typical DSC scans of the PAR and its composites. The area under the melting and crystallization peaks represent the enthalpy of melting, H_m and crystallization, H_c, respectively. The actual values of both thermal parameters are listed in Table I. For the PAR composites, the measured H_m and H_c were corrected with respect to the weight of the fibres. In all cases the crystallization and melting peaks are in the range 183 to 187 °C and 235 to 241 °C, respectively. Table I shows the values of degrees of crystallinity of all the materials examined. In the case of the short glass fibre reinforced PAR, the degree of crystallinity of the matrix in the composites is essentially the same as that of the neat matrix. This indicates that there is no significant change in the morphology of the PAR matrix as a result of the incorporation of glass fibres. A similar observation has been reported by Karger Kocsis and Friedrich [5] for short glass fibre reinforced polyetheretherketone composites. However, in the case of short carbon fibre reinforced PAR slightly higher values of H_m and H_c (hence higher degree of crystallinity) were observed. This may be attributed to the better nucleation ability of carbon fibres as compared to glass fibres. Several studies [9] have indicated that carbon fibres are capable of modifying the microstructure of the surrounding matrices by providing nucleation sites for crystallite growth.

TABLE I DSC results for polyarylamide (PAR) and its composites

Thermal properties	Unit	Neat PAR	Reinforced PAR (vol %)			
			16% GF	27% GF	32% GF	19% CF
Melting peak temperature (T_m)	°C	241.0	240.5	237.4	235.0	236.7
Melt enthalpy (H_m)	J g^{-1}	59.3	56.8	57.2	55.8	63.9
Crystallization peak temperature (T_c)	°C	187.8	189.5	185.8	183.1	184.8
Crystallization enthalpy (ΔH_c)	J g^{-1}	44.3	45.2	42.1	35.7	45.2
Degree of crystallinity (from ΔH_m)	%	45.6	43.7	44.0	42.9	49.2

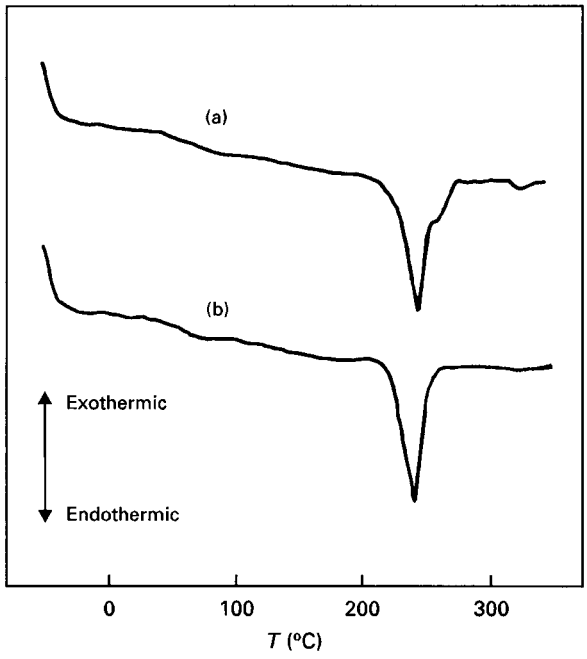

Figure 2 DSC thermograms of (a) neat PAR and (b) PAR composites, respectively, (heating rate: 20 °C min^{-1}).

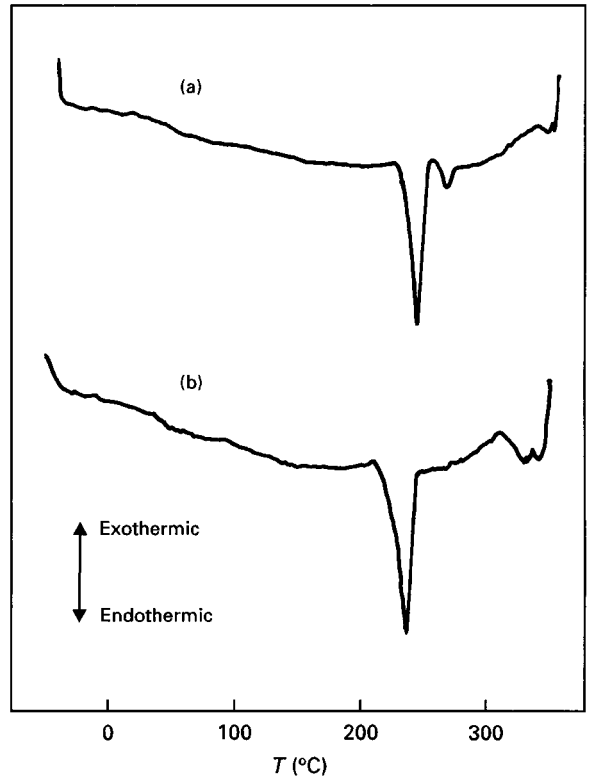

Figure 3 DSC thermograms of (a) neat PAR and (b) PAR composites, respectively, (heating rate: 2 °C min^{-1}).

From the DSC thermogram of the neat PAR shown in Fig. 2 there appears to be a secondary melting peak at a higher temperature, i.e. about 260 °C (as indicated by the arrow). This may be due to the presence of a small amount of another semi-crystalline polymer with a higher T_m than PAR. In order to verify this observation, the DSC run was repeated but at a slower heating rate, i.e. 2 °C min^{-1}. As expected, two distinct melting peaks can be observed, as shown in Fig. 3a. The major peak occurs at 240 °C whilst the minor peak occurs at 260 °C. The occurrence of the minor peak is most probably due to the presence of a small quantity of polyamide 6.6 which was incorporated into PAR matrix to acts as an impact modifier [10]. It is interesting to note that a similar minor peak is not apparent in the case of PAR composites (Fig. 3b). The presence of fibres in the samples will obviously lower the PA6.6 content, hence reduce its contribution to the melting behaviour of PAR.

Fig. 4 shows typical TGA scans of neat PAR and its composites (60 wt % glass fibres). Step analysis of TGA scans of all samples were performed in two stages. The first analysis was carried out in the temperature range 375 to 600 °C under nitrogen while the second one was informed at 600 °C in air. The detailed values of the residual content, as obtained from both analyses, are given in Table II. The higher residual content of PAR composites (ranging from 42 to 66%) as compared to neat PAR (about 14%) at the first step analysis shows that the fibre reinforcements are still thermally stable at such a high temperature. The residual content of 0.54% for neat PAR obtained at the second step analysis clearly indicates that complete decomposition of PAR matrix has been achieved upon subjecting the materials to isothermal heating in air at 600 °C for 10 min. Thus, in the case of PAR composites, the values obtained in step II can be treated as the amount of fibres in the composites. In fact, this

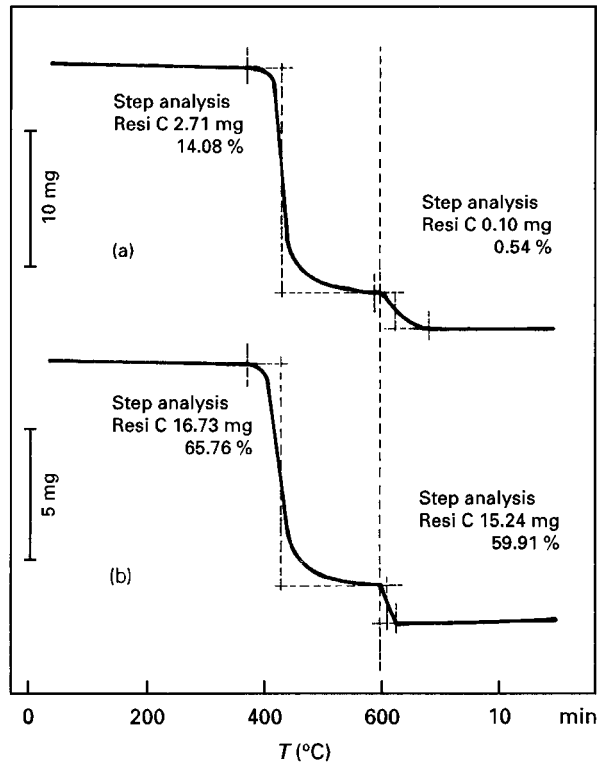

Figure 4 TGA thermograms of (a) neat PAR and (b) PAR composites with 60 wt % GF, respectively.

proved to be in good agreement with the values evaluated by using the burn-off and chemical digestion techniques for both glass and carbon fibres, respectively (Table II).

TABLE II TGA results for polyarylamide (PAR) and its composites

Material	Residual content (%)		Fibre content (wt %)	
	Step I#	Step II*	TGA	Burn-off method
Neat PAR	14.1	0.5	–	–
PAR + 30% GF	43.5	31.3	31.3	29.9
PAR + 50% GF	58.7	50.7	50.7	49.5
PAR + 60% GF	65.8	59.9	59.9	58.5
PAR + 30% CF	41.9	28.2	28.2	29.2+

#Temperature range: ≈ 375 to 600 °C
* Temperature range: ≈ at 600 °C (isothermal)
+ Chemical digestion method

3.2. Kinetics of moisture absorption

Fig. 5 shows the effect of volume fraction of fibres, V_t, on the moisture uptake of PAR at an immersion temperature of 90 °C. The initial linear relationship between M_t and $t^{1/2}$ is clearly observed in each case, followed by saturation. In all cases, good agreement is obtained between the theoretical prediction of Equation 2 (indicated by the solid lines) and the experimental points, which clearly shows that Fickian behaviour is observed. As expected, both glass and carbon fibre reinforced PAR (i.e. at 30 wt % fibres) display a similar trend in their moisture absorption pattern. The values of D and M_m are summarized in Table III. No correction for sample edge effects has been made in the present study, due to the complexity of fibre length and the fibre orientation distributions in the composite system. The values of D obtained are in agreement with the range of values reported by Loos and Springer [8]. According to these workers the values of diffusion coeffecients for most plastics and their composites fall in the range of 10^{-11} to 10^{-12} $m^2 s^{-1}$. From the table, it can be seen that equilibrium moisture content decreases with increasing fibre content and this can be attributed to the decrease in the volume fraction of the hygroscopic

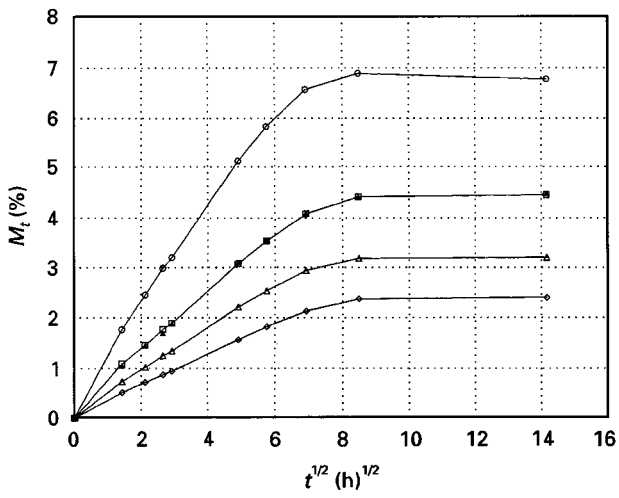

Figure 5 Effect of volume fraction of fibres, V_f on the moisture uptake, M_t of PAR (○) and PAR + (□) 16, (△) 27, (◇) 32 vol % GF and (▲) 19 vol % GF.

TABLE III Effect of fibre volume fractions on the apparent diffusivity, D, and equilibrium moisture content, M_m at 90 °C

Materials	$D \times 10^{-12}$ ($m^2 s^{-1}$)	M_m (%)
Neat PAR	55	6.8
PAR + 16 vol % GF	40	4.4
PAR + 27 vol % GF	32	3.2
PAR + 32 vol % GF	27	2.4
PAR + 19 vol % CF	39	4.5

PAR matrix. In addition, the incorporation of the short fibres has also led to a slight reduction in the apparent diffusivity. This may have been due to the hindrance of the direct moisture diffusion into the polymer matrix as a result of the complex fibre orientation within the composites. The fibre orientation distribution coupled with a broad fibre length distribution can give rise to a discontinuity of the diffusion path in the matrix. A similar trend has been encountered by Mohd Ishak and Berry [11], Mohd Ishak and Lim [12], Mohd Ishak *et al.* [13] and Akay [14] for short carbon fibre reinforced nylon 6.6, short glass fibre reinforced poly(butylene terephthalate) and short glass fibre reinforced nylon 6.6, respectively.

3.3. Fracture toughness

3.3.1. Effect of fibre volume fraction

The load–load line displacement curve ($F - x_{LL}$) obtained from the static fracture test forms the basis for the analysis of the fracture events. Fig. 6 shows the representative load-displacement curves for PAR and its composites tested at 20 °C at a crosshead speed of 1 mm min^{-1}. The curves are indicative of brittle fracture with no evidence of yielding. In the case of the neat PAR sample it is essentially elastically loaded until fracture initiates, marked by a sudden drop in load. This brittle fracture behaviour can be seen clearly from the appearance of the fractured specimen shown in Fig. 7. The neat PAR specimen was broken into three pieces (crack bifurcation). It is believed that the crack bifurcation is related to constraint effects at the notch tip. The detailed discussion on the failure behaviour of PAR will be presented later. As for the PAR composites there is a clear indication of crack propagation taking place after the initiation stage. Its saw-type appearance is related to the repeated crack growth (stick-slip). A similar fracture profile has been reported by Karger-Kocsis and Friedrich [4] in the case of short glass fibre reinforced nylon 6.6 composites. It is worthwhile noting that there are also cases whereby the curve is not monotonic but is discontinuous, i.e. pop-in occurs (Fig. 6b). The curve rises almost linearly, drops in load (pop-in) and then increases again. According to Huang [15] pop-in occurs when crack growth occurs in the interior of the specimen before it occurs at the surfaces. Material inhomogeneity which give rise to a low toughness core and high toughness skin layers may be a possible reason for the pop-in phenomena [16]. In the present study, the pop-in observed did not complicate the analysis of the fracture data.

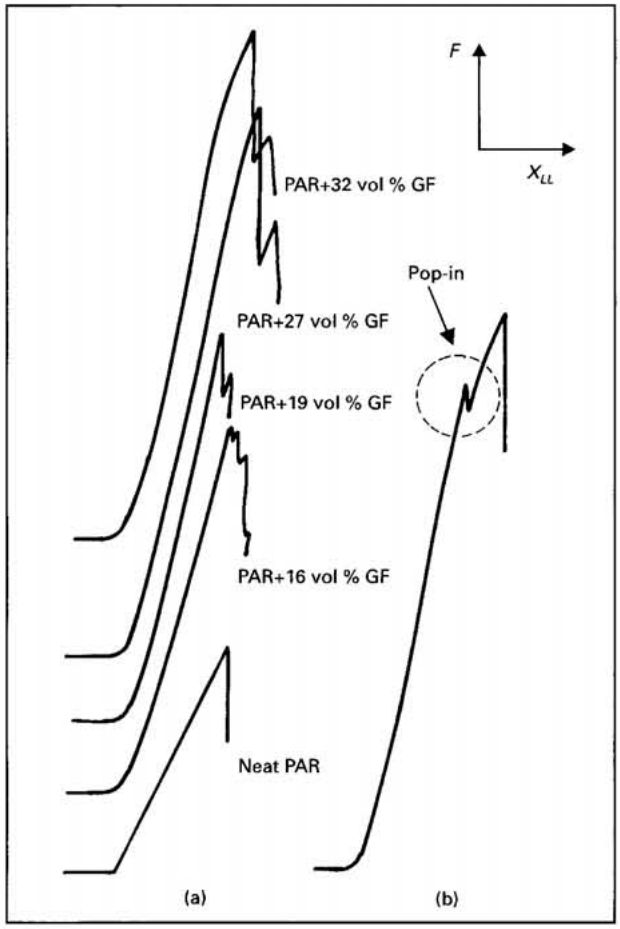

Figure 6 (a) Typical load–load line displacement (F - x_{LL}) profiles of PAR and its composites tested at $T = 20\,^{\circ}C$ and $v = 1\ mm\ min^{-1}$ and (b) the occurrence of pop-in phenomenon in PAR composites.

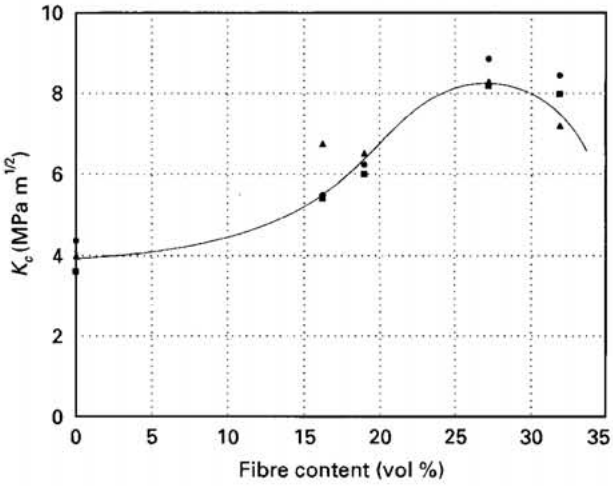

Figure 8 Variation of fracture toughness, K_c with fibre volume fraction, V_f of various PAR composites tested at $T = -40$ (●); 20 (▲) and 80 °C (■) and $v = 1\ mm\ min^{-1}$.

Fig. 8 illustrates the effect of fibre volume fraction, V_f on the fracture toughness, K_c of PAR. It can be seen that incorporation of both short glass and carbon fibres into the PAR matrix has led to much tougher composites. As V_f increases, there are more fibres to blunt, deflect or even to stop the crack propagation. The energy absorbing mechanism not only arises from the energy required to pull-out the fibres from the matrix, and to fracture the matrix, but also the energy dissipated in frictional sliding of one fibre inside the other due to the interaction of fibres. In reviewing the microstructure and fracture mechanical performance of SFRTPs, Karger-Kocsis [17] has noted that both the matrix- and fibre-related micromechanisms are responsible for determining the course of the K_c versus V_f curves. By referring to the equation:

$$K_c = G_c E \tag{3}$$

it can be inferred that K_c will increase with higher fibre content as long as the fibres are able to increase the modulus, E, of the materials sufficiently without leading to significant reduction in the critical strain energy release rate or fracture energy, G_c.

Fig. 9 shows the effect of V_f on the strain energy release rate or fracture energy, G_c, for PAR and its composites. This variation of G_c with V_f is strongly controlled by the occurrence of individual energy absorbing mechanisms during the breakdown of the materials, and their relative effectiveness. As expected, at a fibre loading of 30 wt %, the carbon fibre reinforced PAR possesses higher K_c and G_c values than its glass fibre counterpart. A similar trend has also been observed by Karger-Kocsis [17] on comparing both short glass and carbon fibre reinforced nylon 6.6.

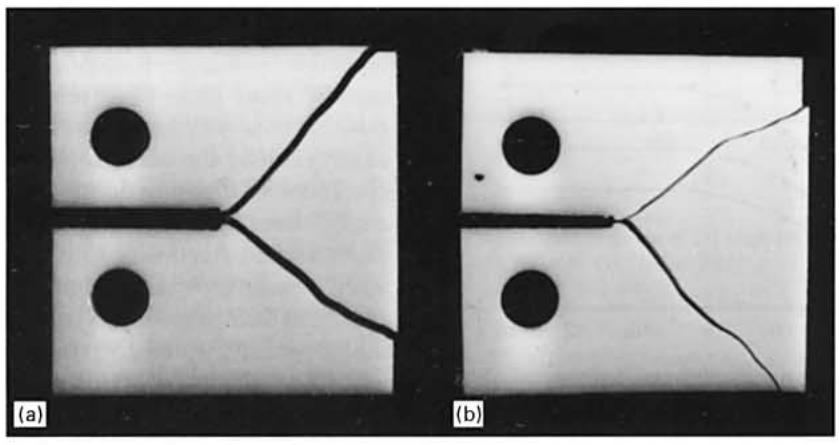

Figure 7 Appearance of the fractured (a) L-T and (b) T-L notched CT-specimen of the neat PAR, tested at $T = 20\,^{\circ}C$ and $v = 1\ mm\ min^{-1}$.

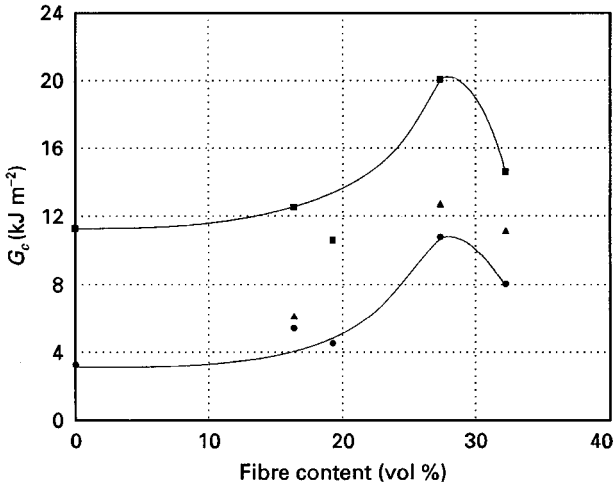

Figure 9 The effect of fibre loadings on the fracture energy, G_c of PAR composites tested at $T = -40$ (●); 20 (▲) and 80 °C (■) and $v = 1$ mm min^{-1}.

3.3.2. Effect of crack direction

Incorporation of short fibres into thermoplastic matrices via melt compounding followed by injection moulding inevitably leads to a mechanical anisotropy of the resulting items. The orientation of the fibres will vary in different layers across the thickness of a specimen, thereby affecting its fracture performance [17]. Thus, it is essential to study the directional dependence of the fracture toughness data.

Table IV shows the variation of K_c with the crack direction of the CT specimens cut from the plaque. At a crosshead speed of 1 mm min^{-1} both L-T (where the crack propagated perpendicular or transverse to MFD) and T-L (where the crack growth parallel or longitudinal to MFD) specimens exhibit a similar trend with regard to the effect of V_f on K_c and G_c. However, at any given V_f, the L-T notched specimens are observed to possess higher K_c and G_c values. This arises as a result of different fibre orientation and layering in the two types of specimens. From Table IV it can be seen that in all cases the ratio of skin layer to specimen thickness ($2S/B$) is much higher than the ratio of the core layer to specimen thickness (C/B). In the case of L-T specimens, fibres in the skin layers are aligned predominantly longitudinal to the load direction, implying higher load bearing capability. On the other hand, in the core layers the fibres are oriented more or less transverse to the loading direction, thus having a lower load bearing capability. This is clearly evident from the SEM micrograph of the fractured surface shown in Fig. 10. This fibre orientation will obviously affect the fibre-related fracture micromechanisms. Fibre fracture, fibre pull-out, fibre/matrix debonding due to matrix shear, and crazing initiated at fibre ends have been proven to operate in the skin layers. On the contrary, in the core layers failure is controlled predominantly by fibre/matrix debonding along the fibre length, accompanied by void and craze initiation at fibre ends [17]. It is obvious that the combination of those failure processes taking place in the skin layer is more energy-consuming that the corresponding processes in the core layers. In the case of T-L specimens, on the other hand, the majority of the fibres in the skin layers are aligned perpendicular to the load direction, thus a much easier crack propagation and a straight path can be expected. In fact this is evident in the present study. The SEM micrograph shown in Fig. 11a was taken from the crack path of the L-T specimen surface. The crack growth followed a zig-zag route according to the fibre avoidance mechanisms. The SEM micrograph taken from the tip region of the stopped crack (Fig. 12a) illustrates clearly the occurrence of fibre/matrix debonding and fibre pull-out. A closer look to the partially opened surface crack (Fig. 12b) provides further evidence that the crack growth is associated with fibre pull-out.

On the contrary, the transverse orientation of fibres (with respect to loading direction) in the skin layers of the T-L specimens results in a normal type of advancing crack profile (Fig. 11b).

3.3.3. Effect of temperature

Fig. 13 illustrates the effect of testing temperature on the load-displacement profiles of PAR and its composites ($V_f = 0.27$). All materials seem to display a similar trend in that the fracture properties are determined by the temperature in a manner which could be

TABLE IV Average values of K_c and G_c for polyarylamide (PAR) and its composites tested at room temperature and at crosshead speeds of 10^0 and 10^3 mm min^{-1}

Material	Loading-notching direction	(C/B)	$(2S/B)$	$v = 10^0$ mm min^{-1}		$v = 10^3$ mm min^{-1}	
				K_c (MPa m$^{1/2}$)	G_c (kJ m^{-2})	K_c (MPa m$^{1/2}$)	G_c (kJ m^{-2})
Neat PAR	LT	–	–	3.6	3.3	0.9	0.3
	TL	–	–	3.6	3.5	0.8	0.2
PAR + 16 vol % GF	LT	0.25	0.75	5.7	5.4	2.2	0.7
	TL	–	–	4.3	3.7	1.9	0.6
PAR + 27 vol % GF	LT	0.31	0.69	8.4	9.9	3.5	1.4
	TL	–	–	6.9	8.0	3.0	1.2
PAR + 32 vol % GF	LT	0.34	0.66	8.0	7.9	3.0	1.1
	TL	–	–	7.4	7.6	3.3	1.2
PAR + 19 vol % CF	LT	0.41	0.59	6.3	4.6	1.6	0.4
	TL	–	–	5.1	3.9	1.9	0.6

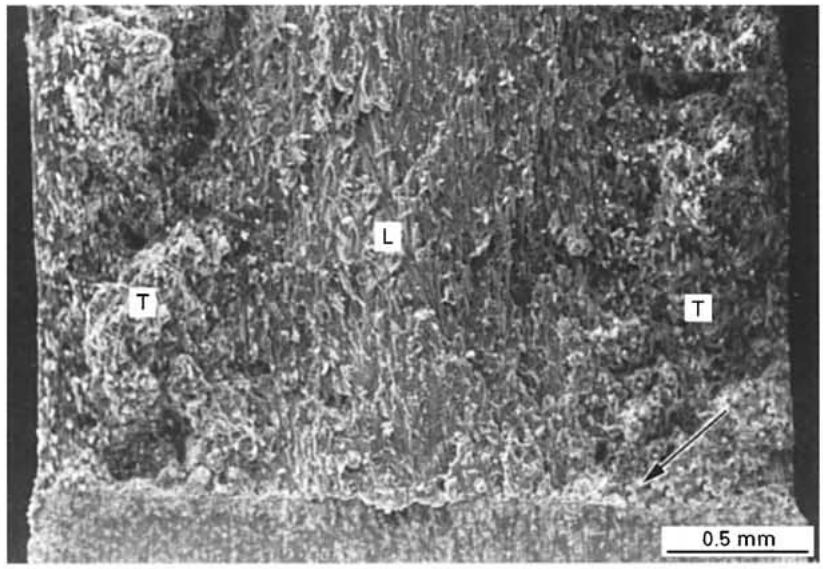

Figure 10 Fracture surface of an L-T-notched CT-specimen of the PAR composite (32 vol % GF). Designations: arrow indicates razor blade notch; T and L denote fibres aligned transverse (T) and longitudinal (L) to the crack plane in the skin (S) and core layers (C), respectively.

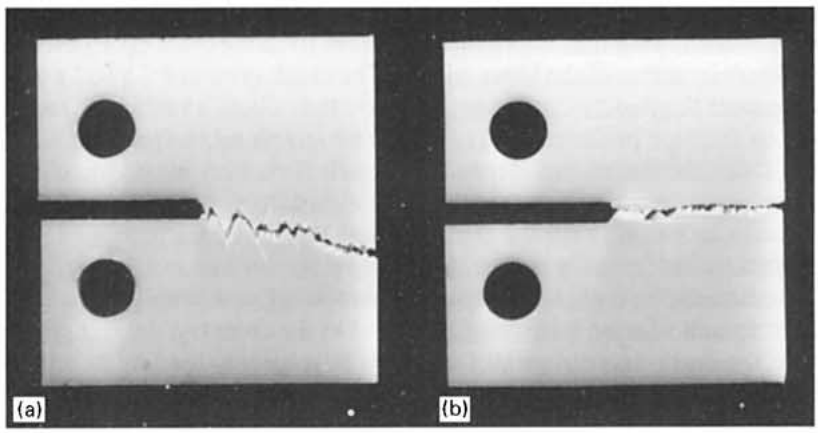

Figure 11 Appearance of the fractured (a) L-T and (b) T-L notched CT-specimen of the PAR composites with 27 vol % GF, tested at $T = 20\,^{\circ}C$ and $v = 1\ mm\ min^{-1}$.

anticipated from the viscoelastic behaviour of PAR. At subambient and room temperatures, the segmental mobility of the polymer chains is frozen-in to the extent that the unreinforced PAR matrix fails in a brittle manner. However, at temperatures above ambient, i.e. 80 °C, some kind of plastic deformation which arises as a result of viscous matrix flow is apparent in the load-deflection curves. The variation of K_c and G_c with temperature is depicted in Figs 8 and 9, respectively. There are no abrupt changes in the values of K_c and G_c for any of the materials tested throughout the temperature range studied. This is not surprising since the DSC analysis studies revealed that PAR has a glass transition temperature of about 70 °C. Thus, one could expect a more significant drop in the fracture parameter if testing were to be carried out at a higher temperature. This has been proven to be the case for PEEK and its composites by Karger-Kocsis and Friedrich [5]. A dramatic reduction in K_c values was observed as the temperature was raised upto 200 °C. However, they also noted that at high temperature, the calculated K_c values no longer fulfill the requirement of linear elastic fracture mechanics (LEFM) theory.

3.3.4. Effect of crosshead speed

The effect of crosshead speed on the fracture parameters of PAR and its composites is shown in Table IV. It can be seen that the fracture properties of both types of materials are strongly influenced by the strain rate. In all cases, both K_c and G_c are drastically reduced as the crosshead speed is increased from 1 to 1000 $mm\ min^{-1}$. This may be attributed to an embrittlement of the matrix under a high velocity condition. This could be expected taking into account the viscoelastic nature of the polymeric materials whereby the segmental mobility of the polymer molecules and the plastic deformation process are very much restricted at high deformation rates. In addition, the contribution of those processes, which are responsible for toughening the composites, such as fibre pull-out

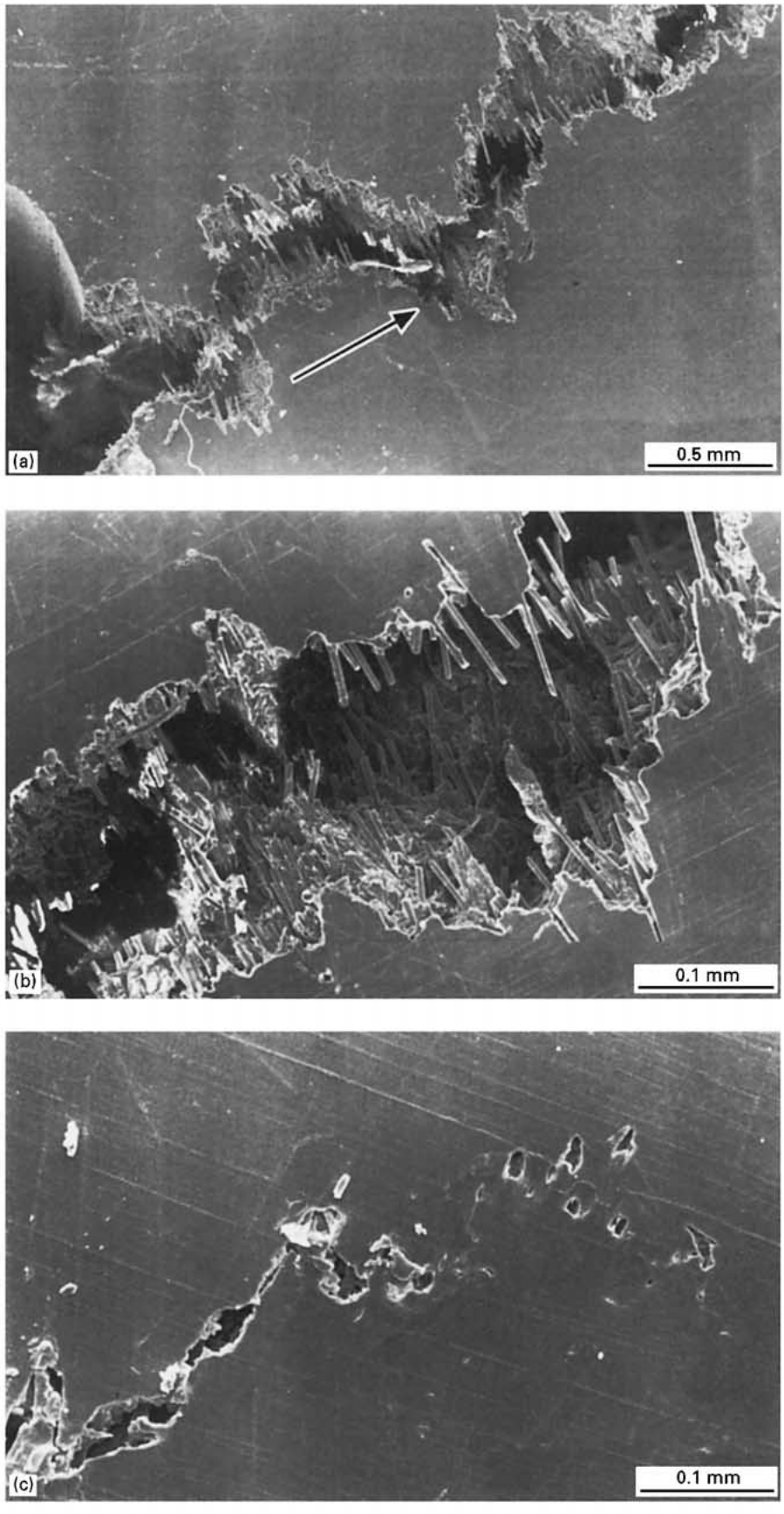

Figure 12 SEM micrographs taken from the surface crack path of an L-T-notched CT-specimen of PAR composite (32 vol % GF), (a) notch region showing both the saw cut and razor blade notch (arrow indicates the crack growth direction), (b) flanks of the opened crack showing the occurrence of fibre pull-out, and (c) region ahead of the surface crack demonstrating fibre debonding and pull-out along with related matrix deformation.

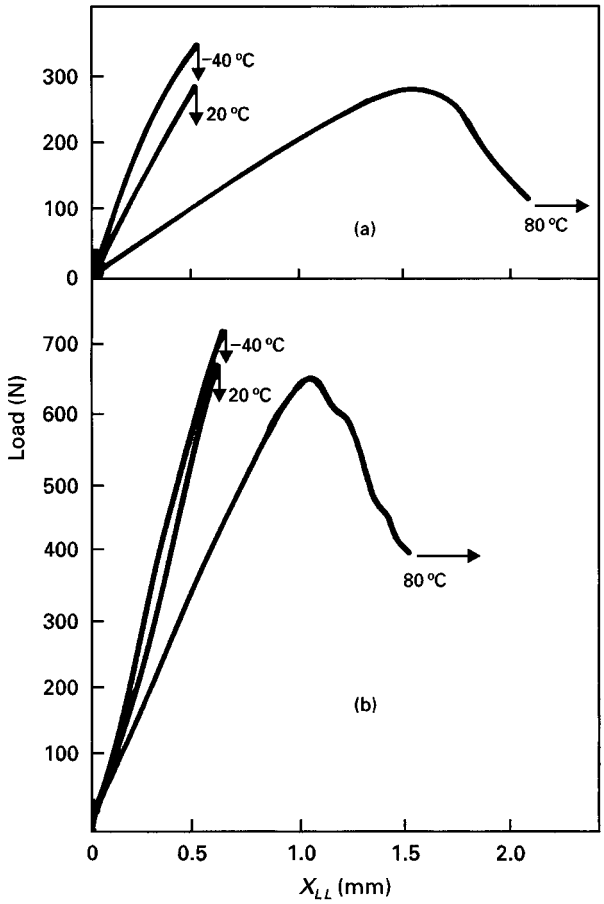

Figure 13 $F - x_{LL}$ curves for L-T-notched CT-specimens of (a) neat PAR and (b) PAR composites with 27 vol % GF, respectively, tested at $T = -40$, 20 and 80 °C and $v = 1$ mm min^{-1}.

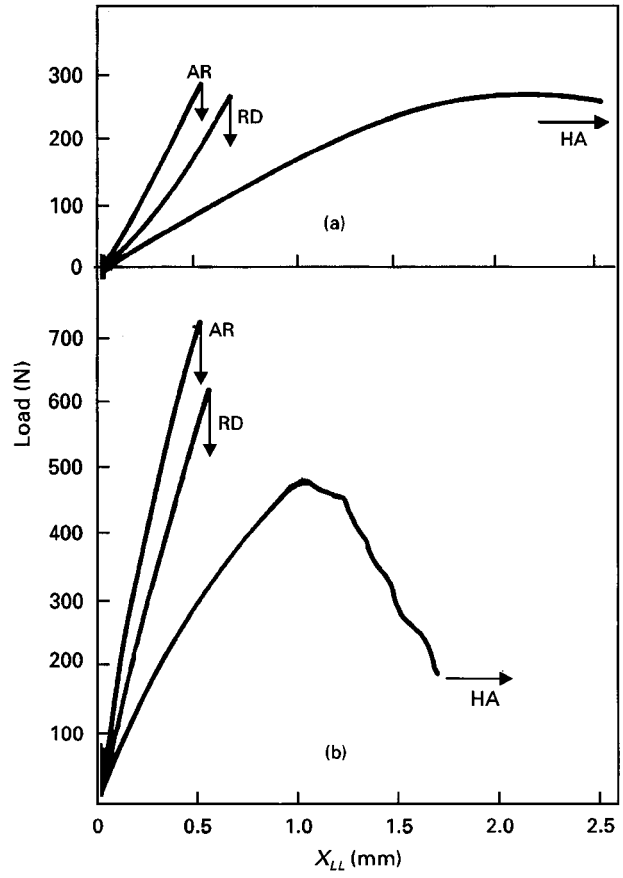

Figure 14 $F - x_{LL}$ curves for L-T-notched CT-specimens of (a) neat PAR and (b) PAR composites with 27 vol % GF, in AR, HA and RD states, respectively.

are greatly suppressed. On the contrary, fracture is dominated by a failure mechanism of lower energy absorption such as brittle fibre-matrix separation and debonding. A similar observation has been reported by other workers for several SFRTP systems [4–6]. Another point worth mentioning is that increasing the crosshead speed has also resulted in a reduction in the directional dependence of the fracture toughness data. With increasing strain rate, the difference in the K_c and G_c values between L-T and T-L specimens decreases, i.e. both types of specimens possessed more or less similar K_c and G_c values. This may be attributed to the nature of the composite breakdown process which becomes more matrix dominated.

3.3.5. Effect of hygrothermal ageing

Fig. 14 shows the load-deflection profiles of PAR and its composites ($V_f = 0.27$). The corresponding curves for the as received or unaged (AR) and the redried (RD) samples are also included for comparison purposes. Generally for HA samples, it can be seen that the presence of moisture has changed the shape of the curves significantly, i.e. the curves appear to be broader together with lower values of the peak or maximum forces compared to the AR counterpart. It appears that the absorbed moisture has significantly changed the mode of fracture of these materials from being brittle to ductile fracture. Both HA PAR and its composites seem to fail in a ductile manner. This is

TABLE V Effect of hygrothermal ageing on the fracture behaviour of PAR and its composites

Materials	As received (AR) (unaged)		Hygrothermal aged (HA) at 90 °C		Redried (RD)	
	K_c (MPa m$^{1/2}$)	G_c (kJ m^{-2})	K_c (MPa m$^{1/2}$)	G_c (kJ m^{-2})	K_c (MPa m$^{1/2}$)	G_c (kJ m^{-2})
Neat PAR	3.6	3.2	1.6*	3.5*	3.5	3.2
PAR + 16 vol % GF	5.7	5.5	4.3	8.3	5.8	6.4
PAR + 27 vol % GF	8.4	9.9	5.3	9.7	7.8	8.4
PAR + 32 vol % GF	8.1	8.3	5.2	7.8	7.3	8.0
PAR + 19 vol % CF	6.4	4.9	5.2	7.7	6.9	5.8

* K_Q values determined by the 5% increased compliance method.

a clear manifestation of the plasticization effects of absorbed water which is fully analogous to that of aliphatic polyamides [7]. the ductile failure of the HA samples is manifested in terms of a reduction of K_c and an enhancement of G_c as indicated in Table V. The ductile matrix failure is also evident from the appearance of the fractured PAR specimens, as shown in Fig. 15b. The specimens were no longer broken

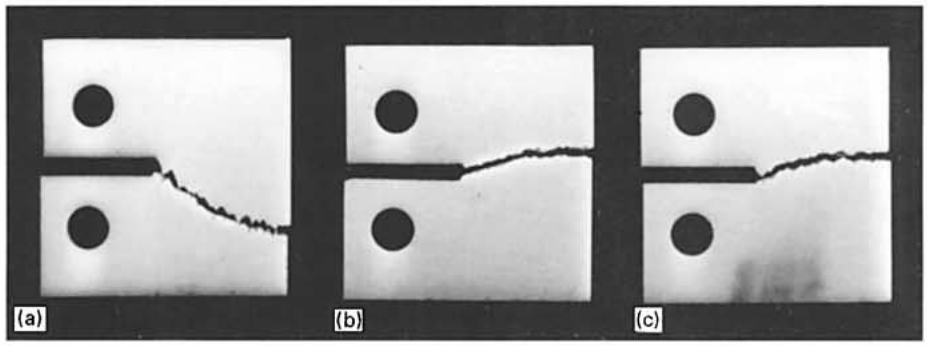

Figure 15 Appearance of the fractured CT-specimens of neat PAR in (a) AR, (b) HA and (c) RD states, respectively.

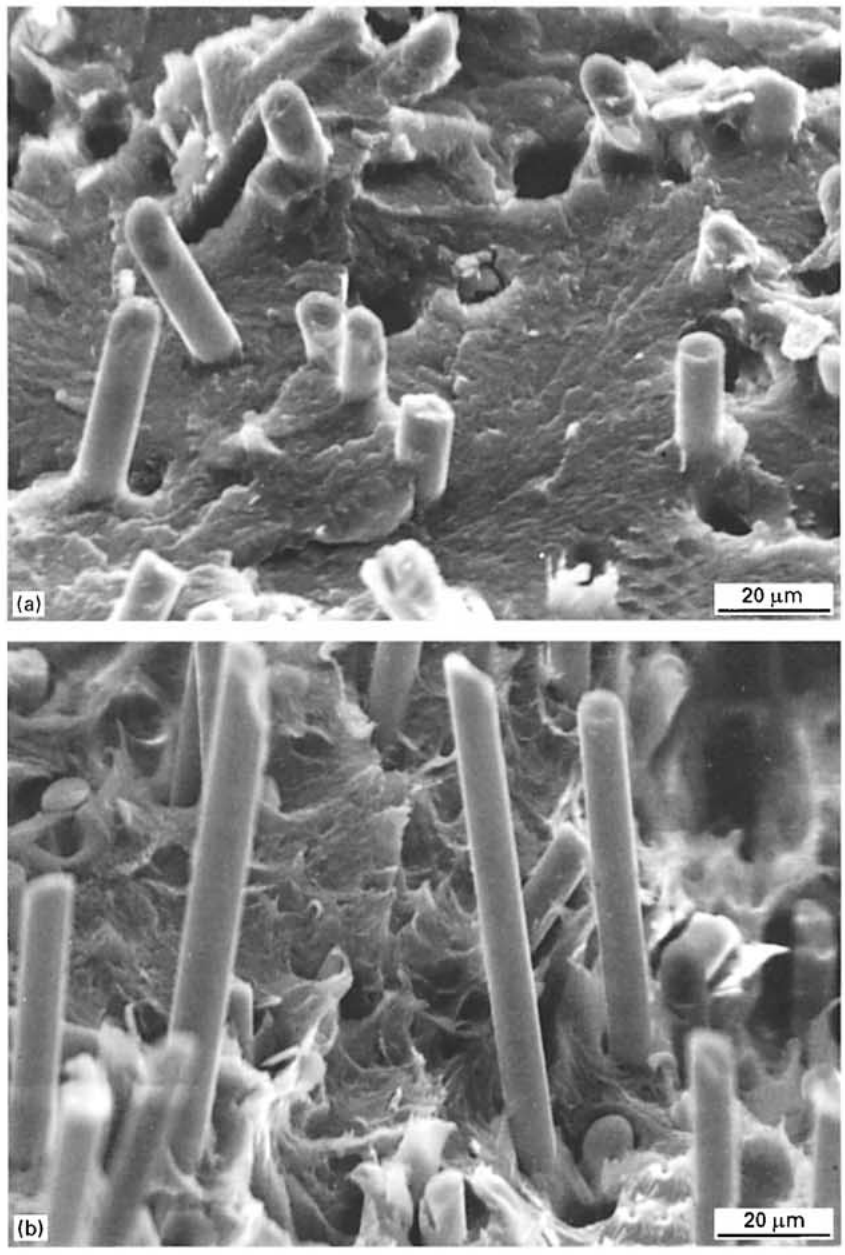

Figure 16 SEM micrographs taken from the fracture surface (S-layer) of an L-T-notched CT-specimen of PAR composites with 16 vol % GF in (a) AR, (b) HA and (c) RD states, respectively.

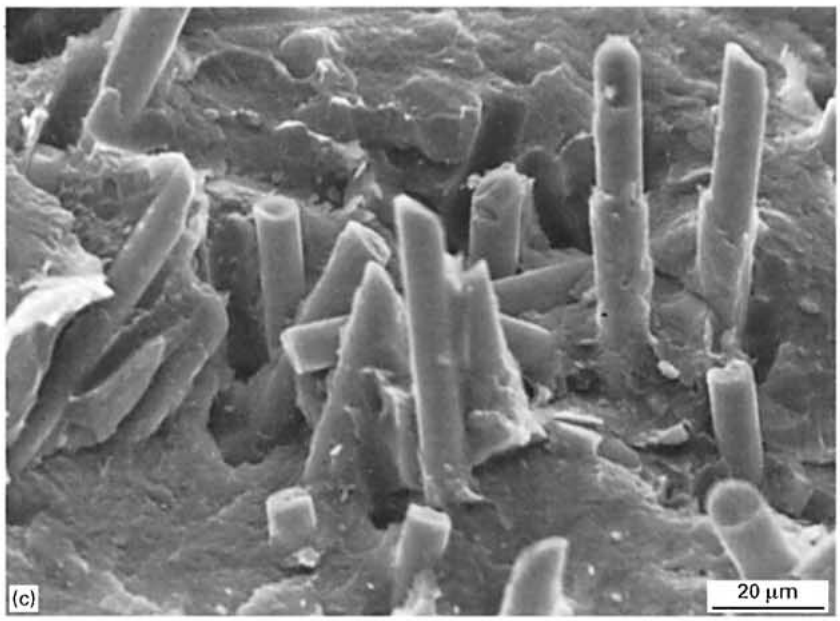

Figure 16 Continued.

catastrophically into three pieces, as in the AR state (Fig. 15a), but instead into just two pieces. This is a clear point that the material constraint in the notch-tip is now released.

The sharp drop in values of K_c for the HA samples may be attributed to the changes in the matrix-and fibre-related micromechanisms. The flexible nature of the polymer molecules in the HA PAR is believed to be the main factor responsible for the ductile failure. In the case of PAR composites, it can be anticipated that the absorbed moisture will not only result in the plasticization effect on the polymer matrix, but also the degradation of the fibre-matrix interface. The moisture attack at the interface will lead to a reduction in the efficiency of stress transfer and ultimately the overall reduction in the load bearing capabilities of the materials. The ductile nature of the PAR matrix and the weak interfacial bonding would then give rise to minimum frictional effects between fibres and matrix during the fibre pull-out process.

This is obvious from the appearance of the fracture surfaces shown by the SEM micrograph in Fig. 16. The matrix seems to be completely detached from the fibres and is viscously stretched into fine tips (Fig. 16b). In addition, the mean fibre pulled out length was considerably longer than in the AR state (Fig. 16a) and the pull-out fibres were bare. The latter supports our claim that water uptake deteriorates the fibre/matrix adhesion and thus promotes fibre debonding and pull out processes. A similar observation has been encountered by Mohd Ishak and Berry [11] for short carbon fibre reinforced nylon 6.6. In a related study, Czigany *et al.* [3] reported that the plasticization of the PAR matrix by water molecules has resulted in the shifting of both the acoustic emission (AE) amplitude and energy curves toward lower values, i.e. where fibre pull-out and debonding dominate. According to these workers, the cumulative AE up to the maximum load may indicate both the water content and fracture mechanical values of the PAR-composites.

Further investigations on the extent of deterioration of the fracture properties of PAR and its composites have been conducted by drying the HA materials. After these CT specimens have reached a constant weight (then assumed to be fully dried), they were subjected to the test. The load-deflection curves obtained are shown in Fig. 14. Excellent recovery of both K_c and G_c were observed in all cases. This clearly indicates that the effect of water is merely as a plasticizer and, on its removal, the fracture properties are almost fully restored. In the case of neat PAR for instance, the catastrophic fracture of CT specimens observed in the AR state were again detected in the RD specimens. As can be seen in Fig. 15c, the RD specimen was broken into three pieces. Comparing the fracture surface of the CT specimens it becomes obvious that the failure mode in the AR (Fig. 16a) and RD states (Fig. 16b) is practically identical. In these states the matrix failed in a brittle manner and the fibre-related individual failure event is dominated by fibre pull-out. The relatively longer pull-out length for the RD specimen can be attributed to the minimal water content of this composite, the fracture of which is accompanied by multiple brittle matrix cracking. Since the glass fibres are at least partially covered by a matrix sheath in both the AR and RD states, one can suppose that the interfacial bonding between GF and PAR matrix is very good.

4. Conclusions

This paper reports on the influence of both internal parameters (volume fraction of fibres, fibre layering) and external parameters (temperature, strain rate and hygrothermal ageing) on the fracture behaviour of injection-moulded polyarylamide (PAR) composites.

The conclusions from this study can be summarized as follows:

1. From the kinetics of moisture absorption study, the absorption process has been observed to follow the prediction of Fick's law, where by the amount of moisture absorbed increases linearly with the square root of time and then gradually slows until a maximum moisture content (M_m) is attained. The values of M_m and diffusion coefficient (D) are determined by the volume fraction of fibres (V_f).

2. The incorporation of both short glass or carbon fibres into the PAR matrix has led to significant improvements in the fracture performance of the composites, the magnitude of which is highly dependent on the microstructure and testing conditions.

3. The water ab- and desorption in PAR composites is a reversible physical process (at least under the experimental conditions used). Thus, the fracture behaviour of the hygrothermally aged (HA) composites can be restored by drying.

4. It was established that short fibre reinforced PAR composites fail by matrix deformation along with fibre/matrix debonding in the crack initiation, whereas fibre pull-out became dominant in the crack propagation zone.

Acknowledgements

Z. A. Mohd Ishak wishes to acknowledge the Marie-Curie Fellowship of the European Union for his stay at the IVW Kaiserslautern, Germany. He also wishes to thank Universiti Sains Malaysia (U.S.M.) for granting the sabbatical leave. The authors are indebted to Dr A. Goldberg (Solvay, Brussels, Belgium) for providing the materials investigated.

References

1. IXEF "Reinforced polyarylamide-based thermoplastic compounds", *Technical Manual*, Solvay S.A, Brussels, Belgium (1989).
2. A. HADDOUT and G. VILLOUTINE, *Composites* **25** (1994) 147.
3. T. CZIGANY, Z. A. MOHD ISHAK and J. KARGER-KOCSIS, *Appl. Compos. Mater.* **2** (1995) 313.
4. J. KARGER-KOCSIS and K. FRIEDRICH, *Compos. Sci. Technol.* **32** (1988) 293.
5. J. KARGER-KOCSIS and K. FRIEDRICH, *Plast. Rubber Compos. Process. Appl.* **8** (1987) 91.
6. J. KARGER-KOCSIS and K. FRIEDRICH, *J. Mater. Sci.* **22** (1987) 947.
7. Z. A. MOHD ISHAK and J. P. BERRY, *Polym. Compos.* **15** (1994) 223.
8. A. C. LOOS and G. S. SPRINGER, *J. Compos. Mater.* **14** (1980) 143.
9. M. J. FOLKES, in "Short fibre reinforced thermoplastics" (Research Studies Press, Wiley, Chichester, 1982).
10. T. O. AHN, S. LEE, H. M. JEONG and S. W. LEE, *Polymer* **37** (1996) 3559.
11. Z. A. MOHD ISHAK and J. P. BERRY, *J. Appl. Polym. Sci.* **51** (1994) 2145.
12. Z. A. MOHD ISHAK and N. C. LIM, *Polym. Eng. Sci.* **34** (1994) 1645.
13. Z. A. MOHD ISHAK, U. S. ISHIAKU and C. P. TAN, in "Advanced New Materials and Emerging New Technologies" edited by P. N. Prasad, J. E. Mark and J. F. Tung (Plenum Publishing Corporation, New York, 1995) p. 134.
14. M. AKAY, *Polym. Polym. Compos.* **2** (1994) 349.
15. D. D. HUANG, *Polym. Compos.* **16** (1995) 10.
16. J. KARGER-KOCSIS, T. HARMIA and T. CZIGANY, *Compos. Sci. Technol.* **54** (1995) 287.
17. J. KARGER-KOCSIS, in "Application of Fracture Mechanics to Composite Materials", edited by K. Friedrich (Elsevier, Armsterdam, the Netherlands, 1989) p. 189.

Received 27 January 1997
and accepted 7 April 1998